

States of an Ensemble of Two-Level Atoms with Reduced Quantum Uncertainty

Monika H. Schleier-Smith, Ian D. Leroux, and Vladan Vuletić

Department of Physics, MIT-Harvard Center for Ultracold Atoms, and Research Laboratory of Electronics, Massachusetts Institute of Technology, Cambridge, Massachusetts 02139, USA

(Dated: October 30, 2018)

We generate entangled states of an ensemble of 5×10^4 ^{87}Rb atoms by optical quantum nondemolition measurement. The resonator-enhanced measurement leaves the atomic ensemble, prepared in a superposition of hyperfine clock levels, in a squeezed spin state. By comparing the resulting reduction of quantum projection noise (up to 8.8(8) dB) with the concomitant reduction of coherence, we demonstrate a clock input state with spectroscopic sensitivity 3.0(8) dB beyond the standard quantum limit.

Atomic clocks [1–3] and atom interferometers [4] are reaching the standard quantum limit (SQL) of precision [1, 5, 6], set by the quantum projection noise inherent in measurements on a collection of uncorrelated particles. In the canonical Ramsey interferometer with N_0 particles, a quantum mechanical phase is converted into occupation probabilities for two states and read out as a population difference N between them. Entanglement can reduce the projection noise ΔN by redistributing it to another variable that does not directly affect the experiment precision. The resulting “squeezed spin state” [7–16] can be used as an input state to an interferometer to overcome the SQL [5, 6, 8, 9].

Formally, the system can be described by an ensemble spin vector $\mathbf{S} = \sum \mathbf{s}_i$ that is the sum over the (pseudo-) spins \mathbf{s}_i of the individual (spin-1/2) particles [5–7]. The ensemble spin S with $\langle \mathbf{S}^2 \rangle = S(S+1)$ can take on values in the range $0 \leq S \leq S_0$, where $S_0 = N_0/2$. For a given S , the minimum variance ΔS_z^2 of $S_z = N/2$ for an unentangled state is realized by the coherent spin state (CSS), and is given by $\Delta S_z^2_{\text{CSS}} = S/2 = |\langle \mathbf{S} \rangle|/2$, where it is assumed that the mean ensemble spin vector $\langle \mathbf{S} \rangle$ lies in the xy -plane. A spin state can be defined as squeezed if it satisfies $\zeta_e \equiv 2\Delta S_z^2/|\langle \mathbf{S} \rangle| < 1$ (entanglement criterion [7, 11]), or $\zeta_m \equiv 2\Delta S_z^2 S_{\text{in}}/|\langle \mathbf{S} \rangle|^2 < 1$ (criterion for metrological gain [5, 6], where S_{in} is the initial spin of the uncorrelated ensemble before the squeezing). ζ_m^{-1} represents the increase in the squared signal-to-noise ratio $|\langle \mathbf{S} \rangle|^2/\Delta S_z^2$ over the value $2S_{\text{in}}$ for the initial uncorrelated state. Since $|\langle \mathbf{S} \rangle| \leq S_{\text{in}}$, we have $\zeta_e \leq \zeta_m$, i.e. metrological gain guarantees entanglement.

The process utilized for spin squeezing can reduce $|\langle \mathbf{S} \rangle|$ below the initial spin S_{in} before the squeezing, thereby reducing the minimum variance ΔS_z^2 that is consistent with an unentangled state [11]. Therefore, measurements of both spin noise ΔS_z and average spin length after squeezing $|\langle \mathbf{S} \rangle|$ are necessary to verify spin squeezing or quantify metrological gain. While reduction of spin noise alone has sometimes been referred to as “spin squeezing” [17, 18] or “number squeezing” [19, 20], we take spin squeezing to require at least demonstrated entanglement, $\zeta_e < 1$, although we are primarily interested in metrological gain, $\zeta_m < 1$.

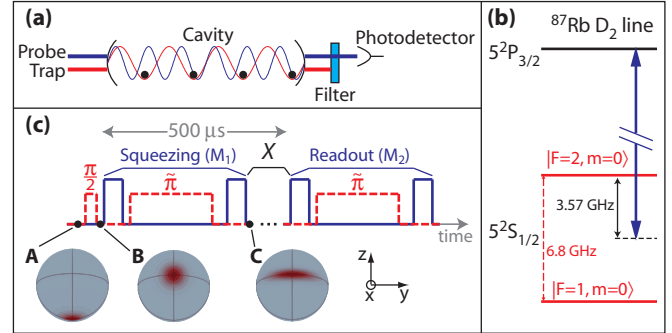


FIG. 1: (a) Experimental setup. (b) Atomic level structure. (c) Experimental sequence. Timing of probe pulses (solid line) and microwave pulses (dashed line) in preparation and readout of a squeezed state. $\tilde{\pi}$ designates a composite π pulse [21]. Various procedures are inserted at X , as described in the text, to measure the CSS variance, measure the noise of a spin component other than S_z , or operate a clock. **A–C** illustrate semiclassical probability distribution functions for the Gaussian states discussed in the text.

Spin noise has been modified by atomic collisions [19, 20, 22] and by absorption of squeezed light [15]. In dilute atomic systems, quantum nondemolition (QND) measurements with light [10–13, 17, 18, 23] have reduced the projection noise of rotating [17] and stationary [18] spins. Spin squeezing has been achieved with two ions [8], and spectroscopic sensitivity further improved with a maximally entangled state of three ions [9]. Recently, spin squeezing with a Bose-Einstein condensate (BEC) in a multiple-well potential has been reported [24]. Demonstrated metrological gains over the SQL include $\zeta_m^{-1} = 3.2(1)$ dB in the three-ion system [9]; $\zeta_m^{-1} \sim 4$ dB by light-induced squeezing within individual atoms of large spin $s = 3$ [25]; and $\zeta_m^{-1} = 3.8(4)$ dB for the BEC [24].

In this Letter, we demonstrate the generation of squeezed spin states of 5×10^4 trapped ^{87}Rb atoms on an atomic-clock transition by resonator-aided QND measurement with a far-detuned light field, as proposed by Kuzmich, Bigelow, and Mandel [10]. We verify the entanglement by comparing the observed reduction in projection noise below that of a coherent spin state (up to

8.8(8) dB) with the accompanying reduction in clock signal, and achieve a 3.0(8) dB improvement in precision over the SQL.

The light-induced spin squeezing presented here requires strong ensemble-light coupling [10, 12–14] (large collective cooperativity [21]). This is achieved by means of a near-confocal optical resonator with, at the $2\pi/k = 780$ nm wavelength of the probe light, a finesse $\mathcal{F} = 5.6(2) \times 10^3$, a linewidth $\kappa = 2\pi \times 1.01(3)$ MHz, and a mode waist $w = 56.9(4)$ μm at the atoms' position, corresponding to a maximal single-atom cooperativity $\eta_0 = 24\mathcal{F}/(\pi k^2 w^2) = 0.203(7)$ [21]. Our experiments are performed on an ensemble containing up to $N_a = 5 \times 10^4$ laser-cooled ^{87}Rb atoms optically trapped inside the resonator in a standing wave of 851-nm light (Fig. 1).

One resonator mode is tuned 3.57(1) GHz to the blue of the $|5^2S_{1/2}, F=2\rangle \rightarrow |5^2P_{3/2}, F'=3\rangle$ transition in ^{87}Rb , such that the atomic index of refraction results in a mode frequency shift ω that is proportional to the population difference $N = N_2 - N_1$ between the hyperfine clock states $|1\rangle = |5^2S_{1/2}, F=1, m_F=0\rangle$ and $|2\rangle = |5^2S_{1/2}, F=2, m_F=0\rangle$. The transmission of a probe laser tuned to the slope of this mode thus directly measures $S_z = N/2$, and is insensitive to total atom number (Fig. 1). The atom-resonator coupling also gives rise to a differential light shift between the clock states, which we use to verify experimentally the coupling strength calculated from first principles from spectroscopically determined resonator parameters. We measure a phase shift of 250(20) μrad per transmitted photon for a maximally coupled atom (on the resonator axis at an antinode of the probe standing wave), in excellent agreement with the calculated value 253(8) μrad [21].

To account for the spatial variation in coupling between standing-wave probe light and atoms, we define an effective atom number $N_0 = (\langle \eta \rangle_e^2 / \langle \eta^2 \rangle_e) N_a \approx 0.66 N_a$, where the single-atom cooperativity η , proportional to the local intensity of probe light, is averaged over the ensemble containing N_a atoms [21]. The definition is chosen so that the projection noise variance of the effective atom number measured via the mode shift $\omega \propto N_a \langle \eta \rangle_e$ satisfies the usual relation $\Delta N_0^2 = N_0$. This avoids carrying near-unity factors through the equations and allows direct comparison to a spatially uniform system of collective cooperativity $N_0 \eta_{\text{eff}}$, where $\eta_{\text{eff}} = (2/3) \langle \eta^2 \rangle_e / \langle \eta \rangle_e = 0.47(1) \eta_0$, taking into account the oscillator strength $2/3$ of the D_2 line and the measured rms transverse cloud radius of 8.1(8) $\mu\text{m} \ll w$. The mode frequency shift per effective atom of population difference N between the clock states is $d\omega/dN = 4.5(2) \times 10^{-5} \kappa$ [21].

To quantify spin squeezing we need to measure ΔS_z^2 and $|\langle \mathbf{S} \rangle|$. The latter can be obtained from the observed contrast \mathcal{C} of Rabi oscillations as $|\langle \mathbf{S} \rangle| = \mathcal{C} S_0$, where the maximum spin $S_0 = N_0/2$ is measured by optically pumping the atoms between the two hyperfine states $F = 1, 2$. For large S_0 the cavity shift ω

exceeds κ ($\omega \leq 1.8\kappa$), which we take into account by correcting for the (accurately measured) Lorentzian line-shape of the resonator. To verify the atom numbers $2S_0$ thus obtained, we have also directly measured the cavity mode frequency shift $\omega \propto S_z$, finding agreement to within 2(4)% [21]. ΔS_z^2 is obtained from transmission measurements that always remain in the linear regime, with $2|\Delta S_z| d\omega/dN \leq 0.01\kappa$.

The probe laser is frequency-stabilized to a far detuned, negligibly shifted mode [21]. Each measurement of S_z employs two probe light pulses of duration $T = 50$ $\mu\text{s} \gg \kappa^{-1} = 158$ ns separated by a 280 μs delay, during which we apply a microwave π pulse sequence [21] to suppress inhomogeneous light shifts (spin echo sequence). Each probe light pulse contains 10^5 to 10^6 photons which, after traversing the resonator, are detected with an overall quantum efficiency $Q_e = 0.43(4)$. From the detected photon numbers in the two pulses, we deduce two cavity shifts ω_{\pm} whose difference constitutes a single measurement M of $S_z = (\omega_+ - \omega_-)/(4d\omega/dN)$. In a typical experiment (Fig. 1(c)), after initializing the ensemble spin state by optical pumping into $|1\rangle$ (**A**) and applying a $\pi/2$ microwave pulse to rotate the CSS into an equal superposition of $|1\rangle$ and $|2\rangle$ (**B**), we perform two measurements M_1 and M_2 to induce and verify conditional spin squeezing. We quantify spin noise ΔS_z by extracting variances from 100 repetitions of such a sequence.

We determine the CSS projection noise level $\Delta S_z^2_{\text{CSS}} = N_0/4$ from the measured atom number N_0 and verify it [5, 6, 15, 17] either by evaluating the variance $\text{Var}(M_1)$ of the set of single measurements M_1 ; or by inserting between two measurements M_1 and M_2 a second CSS preparation, consisting of optical pumping into state $|1\rangle$ and a $\pi/2$ pulse, and evaluating $\text{Var}(M_1 - M_2)/2$. Fig. 2 shows the dependence of the corresponding quantities in atom number units, $y_1 = 4\text{Var}(M_1)$ (open triangles) or $y_2 = 2\text{Var}(M_1 - M_2)$ (open circles), on N_0 . The contribution of CSS projection noise scales as $\Delta S_z^2_{\text{CSS}} \propto N_0$, while atom-number-dependent technical noise, e.g. due to microwave power fluctuations or any sensitivity to atom number fluctuations, generically scales as $\Delta S_z^2_{\text{tech}} \propto N_0^2$. A quadratic fit $y_{1,2} = a_0 + a_1 N_0 + a_2 N_0^2$ yields $a_1 = 1.3(1)$ and $a_2 = 1(2) \times 10^{-6}$ (not shown in Fig. 2), but the data are also well fit by setting $a_1 = 1$, as required by independently measured cavity and atomic properties with no free parameters [21], and allowing a small technical noise contribution $a_2 N_0^2 < N_0$ with $a_2 = 9(3) \times 10^{-6}$ (solid curve). Slow drifts in microwave power of 0.4% over the set of measurements could account for the technical noise of y_1 , which vanishes if the data are analyzed by comparing only adjacent cycles of the experiment [21]. Our ability to prepare an unentangled state close to a CSS—with S_z variance $\Delta S_z^2_{\text{prep}} \sim 1.3S_0/2$ for our largest atom number—is not a prerequisite for spin squeezing but does provide independent confirmation of the CSS reference level for spin noise measurements. We

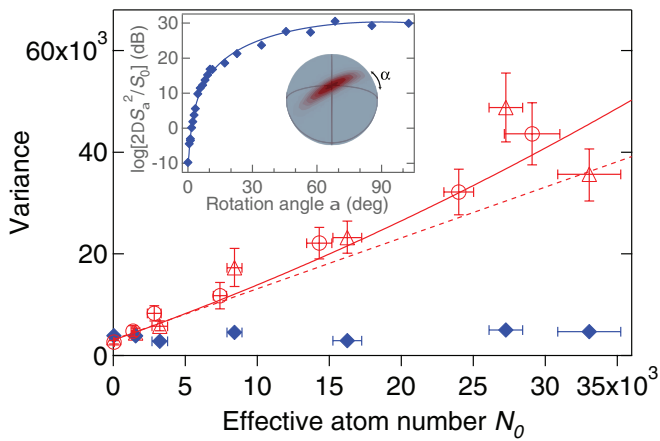


FIG. 2: Spin noise measurements (see text): $y_1 = 4\text{Var}(M_1)$ for a single CSS preparation (open triangles), $y_2 = 2\text{Var}(\tilde{M}_1 - \tilde{M}_2)$ for two independently prepared CSSs (open circles), and $4\Delta S_{z\text{meas}}^2 = 2\text{Var}(M_1 - M_2)$ for two measurements after a single CSS preparation (solid diamonds), all in units of atom number. Vertical error bars are statistical; horizontal error bars indicate standard deviation of measured atom numbers. The solid (dashed) line corresponds to $a_1 = 1, a_2 = 9 \times 10^{-6}$ ($a_2 = 0$). Inset: Variance ΔS_α^2 of S_z after rotating a squeezed state by an angle α about $\langle \mathbf{S} \rangle$, with parameter-free theory curve.

emphasize that, in quantifying spin squeezing below, we conservatively normalize to the CSS noise $4\Delta S_{z\text{CSS}}^2 = N_0$ as obtained from our cavity parameters (dashed line), not to the 30% larger slope of the unconstrained quadratic fit to $y_{1,2}$.

To prepare a state with (conditionally) reduced ΔS_z^2 (Fig. 1(c)C), we simply measure S_z for a CSS on the x -axis with a photon number $p \approx 5 \times 10^5$ sufficiently large to resolve S_z beyond the CSS variance. Each such measurement M_1 yields a value of S_z that is random but known, as verified by a readout measurement M_2 . We plot $2\text{Var}(M_1 - M_2)$ vs. atom number N_0 in Fig. 2 (solid diamonds), finding it a factor of 2 above the photocurrent noise level, with very weak dependence on atom number, and well below the CSS level.

In principle it is possible for the value of S_z at the end of the measurement to differ from the average value of S_z during the measurement. Besides the far-detuned locking light whose effect on S_z is negligible, only spin-echo microwave composite π pulses, whose fidelity was separately measured to be 98(1)%, and probe light are applied during M_1 . The probe light can only change S_z through free-space scattering, which adds at most 3.1(3)% of CSS projection noise at $p = 5 \times 10^5$ [13, 21]. Thus, while the added noise is negligible compared to the CSS level, it can explain part of the small remaining variance of $M_1 - M_2$.

Provided M_1 does not alter the state appreciably, and the measurements M_1, M_2 are identical and uncorrelated [21], $\Delta S_{z\text{meas}}^2 \equiv \text{Var}(M_1 - M_2)/2$ represents the uncertainty of any single such measurement. The conditional

variance of the state after measurement M_1 can then be shown to be $[\Delta S_z^2]_{M_1} = \Delta S_{z\text{prep}}^2 \Delta S_{z\text{meas}}^2 / (\Delta S_{z\text{prep}}^2 + \Delta S_{z\text{meas}}^2)$ [21]. When no new information is gained in measurement M_1 ($\Delta S_{z\text{meas}}^2 \gg \Delta S_{z\text{prep}}^2$), the variance is that of the state preparation process, $\Delta S_{z\text{prep}}^2 \equiv \text{Var}(M_1) - \Delta S_{z\text{meas}}^2$ (close to, but above, the CSS value), while information gained reduces the variance, ultimately to the measurement variance $\Delta S_{z\text{meas}}^2$ of M_1 . At $N_0 = 3.3(2) \times 10^4$ and $p = 6 \times 10^5$, we observe a normalized spin noise $\sigma^2 \equiv [\Delta S_z^2]_{M_1} / \Delta S_{z\text{CSS}}^2 = -9.1(8)$ dB (see Fig. 3); a slight correction for the effect of photon scattering [21] yields $\sigma^2 = -8.8(8)$ dB.

The reduction of $[\Delta S_z^2]_{M_1}$ below the CSS value $\Delta S_{z\text{CSS}}^2$ is accompanied by a substantial increase in ΔS_y^2 because the differential light shift of the atomic levels, corresponding to a rotation of the Bloch vector about the z axis, depends on the intracavity intensity, which in turn depends on S_z . To observe the antisqueezing, we apply a microwave pulse after the squeezing measurement (at X in Fig. 1(c)) to rotate the spin state by a variable angle α about $\langle \mathbf{S} \rangle$ before reading out S_z . The variance ΔS_α^2 of S_z in the rotated state, displayed in the inset to Fig. 2, is a sinusoid that is well described with no free parameters by our model of the ensemble-cavity interaction [21].

To verify spin squeezing, we also need to measure $|\langle \mathbf{S} \rangle|$, observable as the interference contrast $\mathcal{C} = |\langle \mathbf{S} \rangle|/S_0$ of Rabi oscillations induced between measurements M_1 and M_2 . Fig. 3 shows \mathcal{C} as a function of photon number p used in the state-preparation measurement at $N_0 = 4.0(1) \times 10^3$, and we have verified that the contrast \mathcal{C} is independent of atom number [21]. Both normalized spin noise σ^2 and \mathcal{C} can be fit by simple models (dashed and dotted curves) [21]. From these two measurements, we deduce the metrological squeezing parameter ζ_m (solid triangles and solid curve). For $p = 3 \times 10^5$, we achieve $\zeta_m^{-1} = \mathcal{C}^2 / (\sigma^2 \mathcal{C}_{\text{in}}) = 3.0(8)$ dB of metrological gain (and an inverse entanglement parameter $\zeta_e^{-1} = \mathcal{C} / \sigma^2 = 4.2(8)$ dB, not shown). The finite initial contrast $\mathcal{C}_{\text{in}} = S_{\text{in}}/S_0 = 0.7$ in the ensemble without squeezing is due to the resonator locking light, and can be improved by detuning this light further from atomic resonance. The probe-induced contrast reduction probably arises from differential light shifts between the clock states that are imperfectly canceled by the spin echo technique because of atomic motion. In the absence of any technical noise, a fundamental limit to the spin squeezing, associated with photon scattering into free space, would be $\zeta_m^{-1} \leq \sqrt{(3/2)N_0\eta_{\text{eff}}} \sim 18$ dB in our system with cooperativity $N_0\eta_{\text{eff}} \sim 3100$ [13, 14, 21].

For the data presented above, the readout quantifying the entanglement was completed 500 μs after preparation of the squeezed state. We have further verified that the squeezing remains after a Ramsey clock sequence, in which two $\pi/2$ pulses about the x -axis, separated by a short (70 μs) precession time, are inserted at X in Fig. 1c.

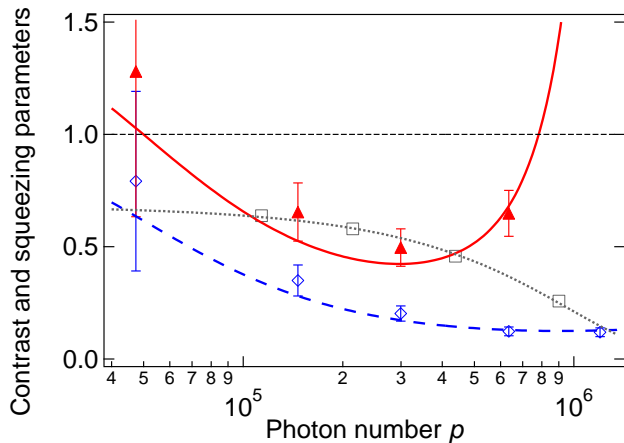


FIG. 3: Measured data with fits of simple models [21] for normalized spin noise $\sigma^2 = [\Delta S_z^2]_{M1} / \Delta S_z^2_{\text{CSS}}$ (open diamonds), contrast \mathcal{C} (open squares), and metrological squeezing parameter ζ_m (solid triangles).

Such a clock can achieve precision below the SQL because the first of these $\pi/2$ rotations initiates it with a phase that is known, from the squeezing measurement, to better than the CSS uncertainty.

The phase coherence time of the unsqueezed CSS in our current trap is 10(2) ms. Both microwave and optical clocks with ~ 1 s coherence times have already been demonstrated with trapped atoms [2, 3, 26–28]. Whether and to what degree the squeezing technique demonstrated here could benefit such clocks and other precision experiments [4] will depend on the clock characteristics, noise sources [16], and lifetime of the squeezed state. These questions, as well as possible systematic effects, need to be investigated in the future.

The group of E. Polzik independently and simultaneously achieved results similar to ours in a Mach-Zehnder interferometer [29]. We have recently demonstrated a new squeezing method using cavity feedback [30].

We thank J.K. Thompson, M.D. Lukin, D. Stamper-Kurn, and E. Polzik for interesting discussions. This work was supported in part by the NSF, DARPA, and the NSF Center for Ultracold Atoms. M. S. acknowledges support from the Hertz Foundation and NSF. I. D. L. acknowledges support from NSERC.

-
- [1] G. Santarelli, P. Laurent, P. Lemonde, A. Clairon, A. G. Mann, S. Chang, A. N. Luiten, and C. Salomon, *Phys. Rev. Lett.* **82**, 4619 (1999).
 [2] A. D. Ludlow, T. Zelevinsky, G. K. Campbell, S. Blatt, M. M. Boyd, M. H. G. de Miranda, M. J. Martin, J. W. Thomsen, S. M. Foreman, J. Ye, et al., *Science* **319**, 1805 (2008).
 [3] M. Takamoto, F.-L. Hong, R. Higashi, and H. Katori,

- Nature* **435**, 321 (2005).
 [4] D. S. Durfee, Y. K. Shaham, and M. A. Kasevich, *Phys. Rev. Lett.* **97**, 240801 (2006).
 [5] D. J. Wineland, J. J. Bollinger, W. M. Itano, F. L. Moore, and D. J. Heinzen, *Phys. Rev. A* **46**, R6797 (1992).
 [6] D. J. Wineland, J. J. Bollinger, W. M. Itano, and D. J. Heinzen, *Phys. Rev. A* **50**, R67 (1994).
 [7] M. Kitagawa and M. Ueda, *Phys. Rev. A* **47**, 5138 (1993).
 [8] V. Meyer, M. A. Rowe, D. Kielpinski, C. A. Sackett, W. M. Itano, C. Monroe, and D. J. Wineland, *Phys. Rev. Lett.* **86**, 5870 (2001).
 [9] D. Leibfried, M. D. Barrett, T. Schaetz, J. Britton, J. Chiaverini, W. M. Itano, J. D. Jost, C. Langer, and D. J. Wineland, *Science* **304**, 1476 (2004).
 [10] A. Kuzmich, N. P. Bigelow, and L. Mandel, *Europhys. Lett.* **42**, 481 (1998).
 [11] A. S. Sørensen and K. Mølmer, *Phys. Rev. Lett.* **86**, 4431 (2001).
 [12] I. Bouchoule and K. Mølmer, *Phys. Rev. A* **66**, 043811 (2002).
 [13] L. B. Madsen and K. Mølmer, *Phys. Rev. A* **70**, 052324 (2004).
 [14] K. Hammerer, K. Mølmer, E. S. Polzik, and J. I. Cirac, *Phys. Rev. A* **70**, 044304 (2004).
 [15] J. Hald, J. L. Sørensen, C. Schori, and E. S. Polzik, *Phys. Rev. Lett.* **83**, 1319 (1999).
 [16] A. André, A. S. Sørensen, and M. D. Lukin, *Phys. Rev. Lett.* **92**, 230801 (2004).
 [17] A. Kuzmich, L. Mandel, and N. P. Bigelow, *Phys. Rev. Lett.* **85**, 1594 (2000).
 [18] T. Takano, M. Fuyama, R. Namiki, and Y. Takahashi, *Physical Review Letters* **102**, 033601 (2009).
 [19] F. Gerbier, S. Fölling, A. Widera, O. Mandel, and I. Bloch, *Phys. Rev. Lett.* **96**, 090401 (2006).
 [20] G.-B. Jo, Y. Shin, S. Will, T. A. Pasquini, M. Saba, W. Ketterle, D. E. Pritchard, M. Vengalattore, and M. Prentiss, *Phys. Rev. Lett.* **98**, 030407 (2007).
 [21] See EPAPS Document No. [number will be inserted by publisher] for further details and supporting experiments. For more information on EPAPS, see <http://www.aip.org/pubservs/epaps.html>.
 [22] C. Orzel, A. K. Tuchman, M. L. Fenselau, M. Yasuda, and M. A. Kasevich, *Science* **291**, 2386 (2001).
 [23] I. Teper, G. Vrijsen, J. Lee, and M. A. Kasevich, *Phys. Rev. A* **78**, 051803(R) (2008).
 [24] J. Estève, C. Gross, A. Weller, S. Giovanazzi, and M. K. Oberthaler, *Nature* **455**, 1216 (2008).
 [25] S. Chaudhury, S. Merkel, T. Herr, A. Silberfarb, I. H. Deutsch, and P. S. Jessen, *Phys. Rev. Lett.* **99**, 163002 (2007).
 [26] D. M. Harber, H. J. Lewandowski, J. M. McGuirk, and E. A. Cornell, *Phys. Rev. A* **66**, 053616 (2002).
 [27] P. Treutlein, P. Hommelhoff, T. Steinmetz, T. W. Hänsch, and J. Reichel, *Phys. Rev. Lett.* **92**, 203005 (2004).
 [28] J. Ye, H. J. Kimble, and H. Katori, *Science* **320**, 1734 (2008), and references therein.
 [29] J. Appel, P. Windpassinger, D. Oblak, U. Hoff, N. Kjaergaard, and E. S. Polzik, *Proceedings of the National Academy of Sciences* **106**, 10960 (2009).
 [30] I. D. Leroux, M. H. Schleier-Smith, and V. Vuletić, *Phys. Rev. Lett.* **104**, 073602 (2010).

States of an Ensemble of Two-Level Atoms with Reduced Quantum Uncertainty: Auxiliary Material

Monika H. Schleier-Smith, Ian D. Leroux, and Vladan Vuletić

*Department of Physics, MIT-Harvard Center for Ultracold Atoms, and Research Laboratory of Electronics,
Massachusetts Institute of Technology, Cambridge, Massachusetts 02139, USA*

(Dated: October 30, 2018)

I. OPTICAL RESONATOR AND DIPOLE TRAP

The parameters of the near-confocal Fabry-Pérot resonator at the wavelengths of trap light (851 nm) and probe light (780 nm) are summarized in table A1. Both trap laser and probe laser are locked to the resonator via Pound-Drever-Hall locks of 1 MHz loop bandwidth. Another feedback loop stabilizes the resonator frequency to an atomic transition in ^{85}Rb .

The atoms are loaded into the standing-wave optical trap from a microchip-based magnetic trap described elsewhere [1]. After polarization gradient cooling in the linearly polarized optical trap, we apply a 5.6 G magnetic field along the resonator axis and a circular polarization fraction of 0.5(1) to the trap light. This combination yields a first-order cancellation of the vector and scalar light shifts, minimizing inhomogeneous broadening of the clock transition. Table A2 summarizes the characteristics of the atomic cloud in the optical dipole trap.

II. DETECTION SETUP

We probe the atoms' index of refraction on the D_2 transition with linear polarization through the optical cavity. The probe laser carrier lies halfway between two TEM_{00} modes of the resonator. A broadband electro-optic modulator (model PM-0K5-10-PFA-PFA-780-UL from EOSPACE) is used to generate sidebands for locking and probing (see Fig. A1). A lock sideband at

113 MHz, resonant with a TEM_{10} mode, produces the Pound-Drever-Hall error signal.

The probe sideband at $(5\omega_{\text{FSR}} + \kappa)/2 \approx 2\pi \times 14080$ MHz lies on the slope of a TEM_{00} resonance with a detuning of $+2\pi \times 3.57(1)$ GHz relative to the atomic $F = 2 \rightarrow F' = 3$ transition. The far off-resonant symmetric (compensation) sideband at $-(5\omega_{\text{FSR}} + \kappa)/2$ lies on the opposite slope of another TEM_{00} mode, such that the total transmission in the two modes is (ideally) sensitive only to atom-induced shifts of the cavity resonance, but not to frequency jitter of the laser relative to the cavity.

The transmitted power in the TEM_{00} mode is coupled into a single-mode fiber to filter out the lock sideband and subsequently detected with overall quantum efficiency $Q_e = 0.43(4)$ on a Si avalanche photodiode (Hamamatsu model S3884). At a typical power of 2 nW for our $T = 50$ μs long probe pulses, the total photodetection noise (including excess noise of the avalanche photodiode operated at gain $M = 13$ [2]) is a factor of 1.9 in variance above the photocurrent shot noise.

III. STATE PREPARATION

Each cycle of the experiment includes three CSS preparations with the same loaded atoms. The first CSS preparation precedes the measurements M_1 and M_2 used to prepare and read out a squeezed state. The measurement M_1 is also used to quantify the unconditional variance of S_z via $y_1 = 4\text{Var}(M_1)$. The two subsequent CSS preparations precede the measurements \tilde{M}_1 and \tilde{M}_2 used for independent verification of the state preparation noise via $y_2 = 2\text{Var}(\tilde{M}_1 - \tilde{M}_2)$.

First CSS preparation: The atoms are optically pumped into $|1, 0\rangle$ using σ_+/σ_- -polarized light on the $F = 1 \rightarrow F' = 0$ transition while repumping on $F = 2 \rightarrow F' = 2$. To improve the state purity, a (composite SCROFULOUS [3]) microwave $\tilde{\pi}$ pulse is subsequently applied on the $|1, 0\rangle \rightarrow |2, 0\rangle$ transition, all $F = 1$ states are emptied using resonant light on the $F = 1 \rightarrow F' = 1$ transition, a second $\tilde{\pi}$ pulse returns atoms from $|2, 0\rangle$ to $|1, 0\rangle$, and all atoms remaining in $F = 2$ ($\sim 12\%$ of the initial atom number) are expelled from the trap using resonant light on the $F = 2 \rightarrow F' = 3$ transition. After this procedure, more than 99% of the remaining atoms are in the state $|1, 0\rangle$. A $\pi/2$ pulse prepares the atoms in

Parameter		$\lambda = 780$ nm	$\lambda = 851$ nm
Mirror separation	L	26.62(1) mm	
Mirror curvature radius	R	25.04(2) mm	
Free spectral range	$\omega_{\text{FSR}}/(2\pi)$	5632.0(2) MHz	
Transverse mode spacing	$\omega_t/(2\pi)$	226.3(3) MHz	
Linewidth	$\kappa_\lambda/(2\pi)$	1.01(3) MHz	135(2) kHz
Finesse	\mathcal{F}_λ	$5.6(2) \times 10^3$	$4.2(1) \times 10^4$
Mode waist	w_λ	56.9(4) μm	59.5(5) μm
Antinode cooperativity	$\eta_{0,\lambda}$	0.203(7)	1.65(4)

TABLE A1: Resonator parameters. The mode waists are calculated at the position of the atoms. Outside this table, all resonator values refer to the probe wavelength $\lambda = 780$ nm.

Optical dipole trap			Atomic cloud		
Axial frequency	$\omega_{\text{ax}}/(2\pi)$	550 kHz	Length	l	1 mm (~ 2000 wells)
Radial frequency	$\omega_r/(2\pi)$	1.8 kHz	RMS radius	σ_r	8.1(8) μm
Trap Depth	U_0/h	24(1) MHz	Radial temperature	$k_B T_r/h$	1.3(2) MHz

TABLE A2: Characteristics of standing-wave dipole trap and atom cloud. The trap depth and trap frequencies are determined from the intracavity power and mode geometry. The radial temperature is measured by suddenly releasing the atoms and observing their ballistic radial expansion as a decrease in coupling to the resonator.

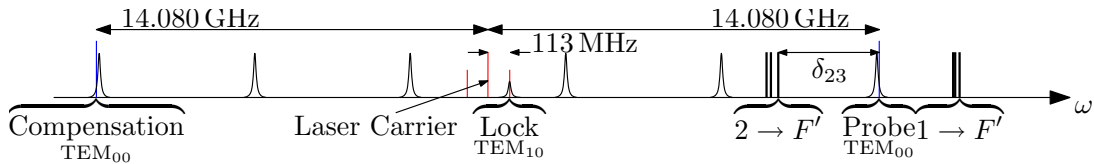


FIG. A1: Laser stabilization and detection scheme, indicating frequencies of carrier and lock sidebands (red) and probe and compensation sidebands (blue) relative to cavity resonances and atomic transitions. Not to scale.

a CSS with $\langle S_z \rangle = 0$, on which the squeezing and readout measurements are performed.

Second and third CSS preparations: We then proceed, using the same loaded atoms, to prepare a CSS in the xy -plane two more times to confirm the CSS projection noise. In order to compare two identically-prepared CSSs with the same total atom number, we forego the state purification procedure described above, since it leads to a $\sim 12\%$ loss of atoms. We thereby allow our imperfect optical pumping to leave 12(2) % of the atoms in $|1, \pm 1\rangle$. These residual atoms do not contribute to our measurement of S_z because our spin echo technique (see Sec. vi) cancels any contribution from atoms not addressed by microwaves resonant with the $|1, 0\rangle \rightarrow |2, 0\rangle$ transition. Therefore, in Fig. 2, the atom number N_0 for the data derived from this pair of preparations (open circles) includes only atoms in $|1, 0\rangle$ and $|2, 0\rangle$ and is systematically 12% lower than the atom number used to measure $\text{Var}(M_1)$ and $\Delta S_{z\text{meas}}^2$ (open triangles and solid diamonds).

State Preparation Noise

Figure 2 indicates the presence of technical noise in the state preparation. The technical noise evident in $\text{Var}(M_1)$ is probably due to slow drifts in microwave power. An alternative analysis, in which we compare each measurement M_1 with the value M_1^{prec} in the preceding experiment cycle, yields a fit $2\text{Var}(M_1 - M_1^{\text{prec}}) = 2650(400) + 0.95(23)N_0 + 1(9) \times 10^{-6}N_0^2$, i.e. a result consistent with no contribution from the quadratic term. We also show in Fig. 2 the variance $y_2 = 2\text{Var}(\tilde{M}_2 - \tilde{M}_1)$, which is immune to slow drifts in microwave power. However, after completing this work, we discovered that the state preparation preceding the measurement \tilde{M}_2 was

compromised by an effect of leakage light during that preparation, to which we attribute the small technical noise observed in y_2 .

IV. ATOM-LIGHT INTERACTION IN AN OPTICAL RESONATOR

We summarize the theory of the interaction of a two-level atom with an optical resonator mode at large detuning $\delta \gg \Gamma$, relative to the excited-state linewidth Γ , from the atomic transition. The extension to our real system of many atoms with nontrivial level structure follows in Sec. v.

A. Atom-Resonator Coupling, Cooperativity, and Optical Depth

The atom-resonator coupling $g(\mathbf{r}) = |\mathbf{d}_{eg} \cdot \mathbf{E}(\mathbf{r})|/\hbar$ for an atom at position $\mathbf{r} = (\rho, z)$ in the Gaussian mode is given by

$$g(\mathbf{r})^2 = d_{eg}^2 \frac{2\omega_{eg}}{\epsilon_0 \hbar \pi w^2 L} e^{-2\rho^2/w(z)^2} \sin^2(kz), \quad (1)$$

where \mathbf{d}_{eg} is the dipole matrix element between the two states $|g\rangle$ and $|e\rangle$, ω_{eg} is the energy of the transition, $w(z)$ is the mode waist at the position of the atom, and L is the resonator length. ($2g$ is the vacuum Rabi frequency.) The coupling $g(\mathbf{r})$ is related to the atomic excited-state linewidth $\Gamma = \omega_{eg}^3 d_{eg}^2 / (3\pi\epsilon_0 \hbar c^3)$ and resonator linewidth κ by the single-atom cooperativity $\eta(\mathbf{r})$, the ratio of the scattering rate into the resonator mode to the free-space scattering rate [4]:

$$\eta(\mathbf{r}) = \frac{4g(\mathbf{r})^2}{\kappa\Gamma} = \frac{24\mathcal{F}}{\pi k^2 w^2} e^{-2\rho^2/w^2} \sin^2(kz), \quad (2)$$

where $\mathcal{F} = \pi c/(L\kappa)$ is the finesse of the resonator and $k = \omega_{eg}/c$ is the probe wavenumber.

The cooperativity is closely related to the resonant optical depth, which for a single atom with scattering cross section σ_{sc} in a uniform beam of area A in free space is given by σ_{sc}/A . A light pulse resonant with the cavity passes through the atomic sample on average $2\mathcal{F}/\pi$ times. For an atom at an antinode of the standing-wave mode, the resonator then enhances the resonant optical depth by a factor of $4\mathcal{F}/\pi$ relative to its value $12/(k^2w^2)$ on the axis of a running-wave Gaussian beam of waist w in free space, so that 2η represents the resonator-enhanced single-atom optical depth.

B. Resonator Mode Shift and Back-Action Phase Shift

We now consider a resonator containing n photons and a single atom in state $|g\rangle$. The shift $\omega_1 = g^2/\delta = \eta\Gamma\kappa/(4\delta)$ of the resonator mode due to the interaction with the atom is accompanied by an AC Stark shift $n\omega_1$ of the atomic level $|g\rangle$ due to the light; the symmetry between these two effects is readily understood in the dressed-atom picture [5]. Since photons are transmitted through the resonator (leaving the resonator in the forward direction) at a rate $n\kappa/2$, the phase shift of the atomic state $|g\rangle$ per transmitted photon is $2\omega_1/\kappa$.

V. POPULATION MEASUREMENT

A. Mode Shift and Effective Atom Number

In Sec. iv, we expressed the shift $\omega_1 = g^2/\delta$ of a resonator mode coupled to a two-level atom in terms of the cooperativity η . In any real atom, at finite detuning, the coupling g is polarization-dependent and must be summed over various excited states. In terms of the cooperativity η of a two-level atom (i.e. the cooperativity on a cycling transition), given by the right-hand side of Eq. 2, a single ^{87}Rb atom at position \mathbf{r} occupying state $|F\rangle$ shifts the mode frequency for linearly polarized light on the D_2 transition by an amount

$$\omega_1^{(F)}(\mathbf{r}) = f\eta(\mathbf{r})\frac{\Gamma\kappa}{4\delta_F}. \quad (3)$$

Here, Γ is the excited-state linewidth; δ_F is an effective detuning from the $|5^2S_{1/2}, F\rangle \rightarrow |5^2P_{3/2}, F'\rangle$ transitions averaged over excited hyperfine states F' ; and $f = \frac{2}{3}$ is the oscillator strength of the D_2 line. For our extended sample of N_a atoms we define the effective cooperativity $\eta_{\text{eff}} = f\langle\eta^2\rangle_e/\langle\eta\rangle_e$ and the effective atom number $N_0 = N_a\langle\eta\rangle_e^2/\langle\eta^2\rangle_e$. Here, $\langle\rangle_e$ denotes an average over the atomic ensemble. This definition, which yields

$N_0 \approx \frac{2}{3}N_a$, is chosen such that the projection noise variance satisfies the usual condition for a uniform sample,

$$\frac{\Delta N_0^2}{N_0} = 1. \quad (4)$$

The mode shift due to an ensemble in state $|F\rangle$ is $\omega^{(F)} = N_0\eta_{\text{eff}}\Gamma\kappa/(4\delta_F)$, where η_{eff} is related to the cooperativity $\eta_0 = 24\mathcal{F}/(\pi k^2w^2)$ of a maximally coupled atom by

$$\frac{\eta_{\text{eff}}}{\eta_0} = f\frac{\langle\sin^4 kz\rangle_e w^2 + 4\sigma_r^2}{\langle\sin^2 kz\rangle_e w^2 + 8\sigma_r^2} = 0.47(1) \quad (5)$$

for our cloud of radius $\sigma_r \ll w$.

B. Measurement of S_z

The probe sideband is tuned to the frequency between the $|5^2S_{1/2}, F=1\rangle \rightarrow |5^2P_{3/2}\rangle$ and $|5^2S_{1/2}, F=2\rangle \rightarrow |5^2P_{3/2}\rangle$ transitions at which the atom-induced differential frequency shift between the probe and compensation sidebands,

$$\omega = \frac{(N_2 - N_1)\eta_{\text{eff}}\Gamma\kappa}{4\delta'}, \quad (6)$$

is proportional to the effective-atom population difference $N = N_2 - N_1$ between the hyperfine states $F=1, 2$, but independent of the total atom number $N_1 + N_2$. Here $\delta' = 2\pi \times 3200(10)$ MHz; see Table A3 for details. For our cloud geometry and probe polarization, the differential mode shift per effective atom is $d\omega/dN = 2\pi \times 45(1)$ Hz/atom $= 4.5(2) \times 10^{-5}$ κ /atom. The mode shifts due to projection noise on N are much smaller than $\kappa/2$, leaving the resonator transmission in the linear regime, such that the change in transmitted power is directly proportional to $S_z = N/2$. Nevertheless, in all measurements of S_z we take into account the full Lorentzian lineshape of the resonator transmission, allowing the same procedure to be used for measuring projection noise, contrast, and total atom number. The cavity linewidth $\kappa/(2\pi) = 1.01(3)$ MHz at the probe wavelength is accurately measured by tuning the probe sideband over the TEM₀₀ resonance of the empty cavity and measuring probe transmission.

C. Measurement of N_0

At the end of each experiment cycle, we measure the effective atom number N_0 . We determine the atom number by pumping all atoms first into $F=2$, then into $F=1$, and in each case measuring the resonator transmission. Although the resonator mode shifts $\omega^{(F)}$ are linear in N_0 , they are on the order of κ for our typical

Resonance	$\delta_{23}/(2\pi \text{ GHz})$	Cavity Shift per Effective Atom/ $(\kappa \times 10^{-6})$	
		$ F = 1, m_F = 0\rangle$	$ F = 2, m_F = 0\rangle$
Probe	3.57(1)	-49(2)	+39(1)
Lock	-10.40(1)	-0.6(1)	-1.0(2)
Compensation	-24.59(1)	-4.6(2)	-5.8(2)

TABLE A3: Frequency shifts per effective atom in either of the clock states for relevant resonator modes. δ_{23} is the detuning of the given mode from the $|5^2S_{1/2}, F = 2\rangle \rightarrow |5^2P_{3/2}, F' = 3\rangle$ atomic transition. The calculated shifts include the excited-state hyperfine structure, as well as the spatial overlap of the cloud with the mode.

atom numbers, so that the transmitted power is a non-linear function of $\omega^{(F)}$ which we must invert to obtain the atom number. To verify our determination of the resonator shift from the non-linear transmission signal, we additionally measure the average mode shift over several cycles of the experiment by finding the probe sideband frequencies $\omega_p^{(F)}$ that maximize the probe transmission when all atoms are pumped into hyperfine state F . By thus directly measuring the mode frequency shift, we obtain a linear measure of effective atom number $N_0^L = (\omega_p^{(2)} - \omega_p^{(1)})/2/(2\pi \times 45 \text{ Hz})$. In Figure A2 we plot N_0^L against the average atom number N_0 extracted from the nonlinear transmission signal. The fit $N_0^L = 0.98(4)N_0$ with reduced $\chi^2 = 0.3$ indicates that the two measurements are in good agreement.

At the large atom number $N_0 = 3.3(2) \times 10^4$ where we calculate squeezing parameters, the dominant uncertainty in N_0 arises from sensitivity to the initial placement of the probe and compensation sidebands. In extracting N_0 from the transmission, we assume that we have correctly placed the probe and compensation sidebands at $\pm\kappa/2$ detuning from cavity resonance when $S_z = 0$. We monitor the placement of the sidebands in each cycle of the experiment by shifting the frequency of the laser relative to the resonator by $+\kappa$ and $-\kappa$ from the usual configuration and measuring the transmission in each case. Hence, we are confident that any systematic error in the placement of these sidebands is less than the shot-to-shot fluctuations. We therefore always estimate the uncertainty in N_0 by the standard deviation of the calculated N_0 values.

D. Experimental Verification of Atom-Resonator Interaction

The calculated mode shift per atom, Eqs. 3 and 6, is used to convert measured transmission into atom number. We verify it by measuring the complementary atomic phase shift $\phi = 2(\omega_1^{(2)} - \omega_1^{(1)})/\kappa$ induced between states $|1\rangle$ and $|2\rangle$ by a single probe photon transmitted through the resonator. We determine the phase shift ϕ_0 of a maximally-coupled atom by means of a Ramsey measurement [6], applying an optical probe pulse of variable

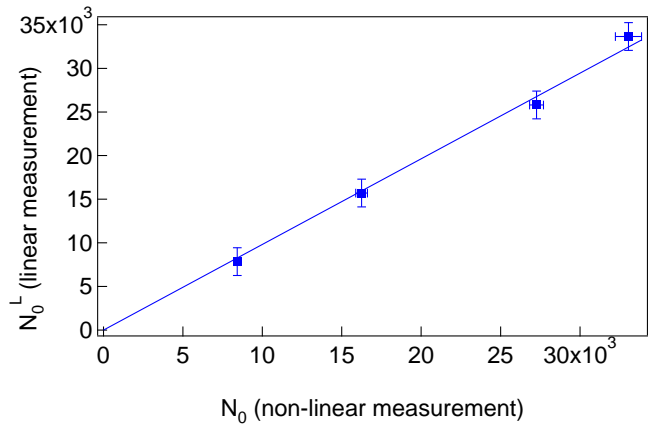


FIG. A2: Comparison of two methods of determining effective atom number, as described in the text. The vertical error bars indicate the uncertainty in positioning the probe sideband on cavity resonance. The horizontal error bars arise because the atom number N_0 is the average over a different set of loading cycles from those in which N_0^L is measured.

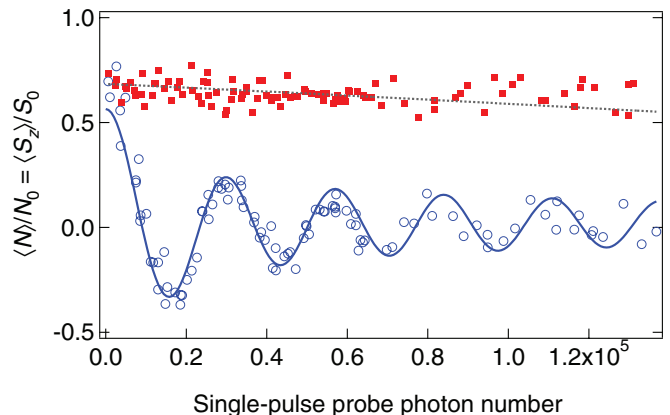


FIG. A3: Measurement of the atom-photon interaction. A probe pulse of varying photon number p is inserted into a Ramsey sequence, resulting in a differential light shift between atomic states. The light-induced phase shift and decoherence (open circles) can be suppressed by a spin echo technique where a microwave π pulse is inserted between two probe pulses (solid squares).

duration between two microwave $\pi/2$ pulses. The population difference $2S_z$, measured via the resonator shift (Fig. A3), is an oscillatory function of the transmitted probe photon number p . The oscillation is damped due to inhomogeneous light shifts. For an ensemble of atoms on the resonator axis evenly distributed with respect to the probe standing wave, a spin state prepared along the x -axis of the Bloch sphere acquires, after the interaction,

$$\begin{aligned} \langle S_x \rangle_e &\propto \frac{\int_0^{2\pi} \cos(p\phi_0 \sin^2(kz)) \sin^2(kz) dz}{\int_0^{2\pi} \sin^2(kz) dz} \\ &= J_0(u) \cos(u) - J_1(u) \sin(u), \end{aligned} \quad (7)$$

where the J_n are Bessel functions of the first kind and $u = p\phi_0/2$. From a fit of this form we extract $\phi_0 = 230(20)$ μrad . (The phase shifts due to lock and compensation light are negligible.) A fit to a full numerical model including the radial cloud size yields $\phi_0^{\text{meas}} = 250(20)$ μrad , in excellent agreement with the value $\phi_0^{\text{calc}} = 253(8)$ μrad calculated from cavity parameters.

VI. SPIN ECHO SEQUENCE

We use a spin echo technique to reduce the probe-induced inhomogeneous broadening (Fig. A3). All probe light is applied in two 50 μs long pulses separated by a composite $\tilde{\pi}$ pulse, consisting of a sequence $R_{\pi/3}(\pi)R_{-\pi/3}(\pi)R_{\pi/3}(\pi)$ of three simple microwave π pulses, where the subscripts indicate phases chosen to compensate variations in pulse area [7]. The spin echo is optimized at a probe pulse separation of 330(20) μs , corresponding to a half-period of the radial trap oscillation.

VII. DATA ANALYSIS

A. Noise Model

The spin measurement variance $\Delta S_{z\text{meas}}^2 = \text{Var}(M_1 - M_2)/2$ as a function of probe photon number p used in the measurement (Fig. A4) is well described by assuming the following independent noise contributions to $4\Delta S_{z\text{meas}}^2 = b_{-2}p^{-2} + b_{-1}p^{-1} + b_0p^0 + b_1p^1$: electronic noise of the detector scaling as $\Delta S_{z\text{meas}}^2 \propto p^{-2}$; photon shot noise and avalanche excess noise scaling as $\Delta S_{z\text{meas}}^2 \propto p^{-1}$; technical noise that is independent of photon number, including the effects of imperfect microwave rotations in the spin echo procedure; and noise due to photon (Raman) scattering, $\Delta S_{z\text{meas}}^2 \propto p$. We quantify each of the known noise contributions:

- **Photon shot noise and avalanche excess noise:** We calculate the photocurrent noise due to the probe and compensation light, taking into account both the shot noise of the light detected

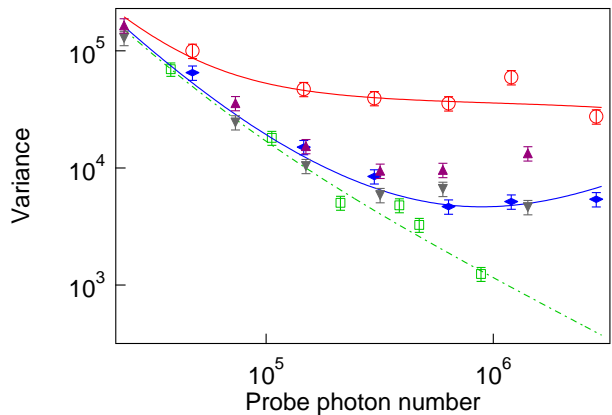


FIG. A4: Comparison of observed variances with noise model. Shown as a function of probe photon number p are the measurement variance in atom number units, $4\Delta S_{z\text{meas}}^2 = 2\text{Var}(M_1 - M_2)$, with (solid blue diamonds) and without (open green squares) atoms; and the variance $4\text{Var}(M_1)$ with atoms, which includes projection noise. In addition, variances $2\text{Var}(M_{1+} - M_{2+})$ (solid gray inverted triangles) and $2\text{Var}(M_{1-} - M_{2-})$ (solid purple triangles) using a single probe pulse from each measurement (as shown in Fig. A5) are plotted as a function of single-pulse probe photon number $p/2$. Curves correspond to the noise model described in Sec. A.

with a quantum efficiency $Q_e = 0.43(4)$ and the excess noise factor $f_{\text{APD}} = 1.9(4)$ of the avalanche photodiode operated at a gain of 13 [2], obtaining $b_{-1} = 2(f_{\text{APD}}/Q_e)(dN/d(2\omega/\kappa))^2 = 1.1(3) \times 10^{-9}$.

- **Electronic noise:** From a fit to the noise measured in the absence of atoms (open green squares in Fig. A4) in which we constrain the coefficient b_{-1} to the value calculated above, we obtain an electronic noise contribution $b_{-2} = 6(1) \times 10^{13}$, most of which is attributable to the Johnson noise of the transimpedance gain resistor in the photodetection circuit.
- **Microwave infidelity:** The $\tilde{\pi}$ pulse used in the spin echo produces at least 98(1)% inversion. We model the imperfect $\tilde{\pi}$ pulse as a perfect one combined with an incoherent process that flips on average $\mu = 2(1)\%$ of the spins, yielding $b_{0,\mu} = \mu N_0$. We treat the errors as incoherent because the atomic phase is inhomogeneously broadened by $(\phi_0/2)p = 1.3 \times 10^{-4}p$ radians when the microwaves are applied. At the optimum photon number $p = 3 \times 10^5$ for squeezing, the Ramsey contrast remaining after a single probe pulse is only 10(3)% (see Fig. A3). We briefly address possible coherent noise processes below (Sec. A), placing an upper bound on the effect of such processes.
- **Raman scattering:** In our system, the probability of a Raman scattering event is $P_{\text{Ram}} = 5.6 \times 10^{-8}$ per probe photon transmitted through

the resonator. This value, calculated including the full excited-state and ground-state hyperfine structures, includes probabilities $P_{\text{Ram}} = P_{\Delta F} + P_{\Delta m_F} + P_{\Delta F \Delta m_F}$ corresponding to three types of scattering events: those which change F but not m_F , those which change m_F but not F , and those which change both F and m_F , respectively. To first order in these probabilities, the total contribution of Raman scattering to the measurement variance is $b_1 = (4/3P_{\Delta F} + 1/2P_{\Delta m_F} + 1/3P_{\Delta F \Delta m_F})N_0 = 4.7 \times 10^{-8}N_0$ per probe photon. Section A outlines the derivation of this expression for b_1 .

Figure A4 shows a fit of the above model (solid blue curve) to the observed measurement variance in atom number units, $4\Delta S_{z\text{meas}}^2$, at $N_0 = 3.3(2) \times 10^4$ and variable photon number p (solid blue diamonds). We fix the noise contributions enumerated above and leave free a term $b_{0,\text{tech}}$ to account for technical noise that is independent of probe photon number but not due to microwave infidelity. The value $b_{0,\text{tech}} = 1400(400) = 0.04(1)N_0$ obtained from the fit may be due to frequency jitter of the laser relative to the cavity that is incompletely canceled by the compensation sideband; or to technical noise in the probe light level, e.g. from fluctuations in the coupling of the light to the cavity. The data show very good agreement with our noise model with this single free parameter $b_{0,\text{tech}}$, all other parameters being independently measured or calculated as described above.

The distinction between the two contributions to $b_0 = b_{0,\text{tech}} + b_{0,\mu}$ is verified by also plotting measurement variances (in atom number units) $2\text{Var}(M_{1-} - M_{2-})$ and $2\text{Var}(M_{1+} - M_{2+})$ obtained by comparing either the first and last or the second and third of the four probe pulses $M_{i\pm}$ constituting the two measurements M_i , $i \in \{1, 2\}$; see Fig. A5. Whereas two $\tilde{\pi}$ pulses are applied between M_{1-} and M_{2-} , no microwaves are applied between M_{1+} and M_{2+} . Thus, fits (not pictured) to $2\text{Var}(M_{1-} - M_{2-})$ and $2\text{Var}(M_{1+} - M_{2+})$ reveal the microwave infidelity $\mu_{\text{fit}} = (b_0^- - b_0^+)/ (4N_0) = 0.03(1)$, consistent with the independently determined value $\mu = 0.02(1)$. (The value μ_{fit} also includes a small contribution < 0.01 due to photons scattered by the lock light.)

In addition, we plot $4\text{Var}(M_1)$ (open red circles in Fig. A4) and a curve given by the following expression: $4\text{Var}(M_1) = b_{-2}/p^2 + b_{-1}/p + b_{0,\text{tech}/\text{prep}} + (1 - \mu - [2P_{\Delta F}/3 + P_{\Delta m_F}/2 + 2P_{\Delta F \Delta m_F}/3]p)N_0$ (see Sec. A). Here, we fit the term $b_{0,\text{tech}/\text{prep}} = 0.14(7)N_0$ to allow for technical noise in the state preparation but constrain all other parameters to the values given above.

The red curve in Fig. 3 is derived by combining the fits to $4\Delta S_{z\text{meas}}^2$ and $4\text{Var}(M_1)$ described above with a fit to the contrast, described in Sec. D, in accordance with Eq. 15 below. The dashed blue curve in Fig. 3 corresponds to the same expression without the contrast factors.

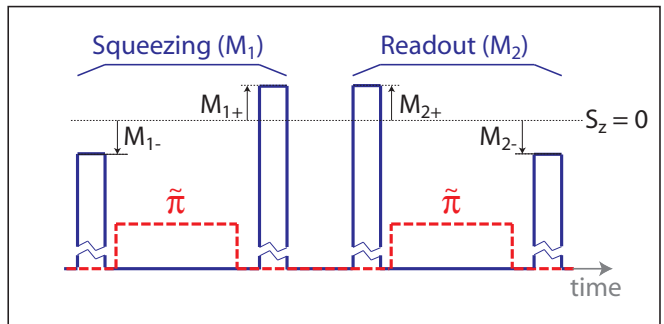


FIG. A5: Measurements M_1 and M_2 of S_z for spin squeezing and readout. Each measurement is obtained from the probe light transmitted (solid blue line) in two pulses, before and after applying microwaves (dashed red line) to perform a $\tilde{\pi}$ rotation. Specifically, each measurement can be expressed as the average $M_i = (M_{i+} + M_{i-})/2$ of two single-pulse measurements $M_{i\pm} = \pm\omega_{i\pm}/|2d\omega/dN|$, where $\omega_{i\pm}$ are the atom-induced shifts of the cavity resonance deduced from the transmitted probe light. With each $\tilde{\pi}$ rotation, we switch the sign convention for $S_z = \pm(N_2 - N_1)/2$ to compensate for the population exchange between states $|1\rangle$ and $|2\rangle$.

Bound on Coherent Microwave Errors

We have noted above that any noise process associated with coherent microwave pulse errors in the spin echo is highly suppressed by inhomogeneous broadening of the atomic phase before the spin-echo-induced rephasing. For example, the drifts of 0.4% in microwave power (0.2% in Rabi frequency) which we infer from our state preparation noise $\Delta S_{z\text{prep}}^2$ would lead to rotation errors substantially less than $\delta\phi_{\text{max}} = 2 \times 10^{-3}\pi$ in our composite $\tilde{\pi}$ pulse, which is designed to compensate for microwave power errors. At the optimum squeezing photon number $p = 3 \times 10^5$, where the interference contrast is $C_{\text{SE}} \approx 10\%$ when the spin-echo microwaves are applied (see Fig. A3), the resulting normalized variance in S_z would be at most $\Delta S_{z\text{coh}}^2 / \Delta S_{z\text{CSS}}^2 < \delta\phi_{\text{max}}^2 C_{\text{SE}}^2 N_0 = 4 \times 10^{-7}N_0 \approx 0.01$ at $N_0 = 33000$. This is much smaller than the normalized spin noise $[\Delta S_z^2]_{M_1} / \Delta S_{z\text{CSS}}^2 = 0.20(3)$ at the same photon number.

Note further that, while the calculation of conditional spin noise from the spin measurement variance $\Delta S_{z\text{meas}}^2 = \text{Var}(M_1 - M_2)/2$ obscures measurement errors that are perfectly correlated, it overestimates by a factor of two the effect of measurement errors that are perfectly anticorrelated. Since correlated microwave errors can yield either correlated or anticorrelated measurement errors depending upon the atomic phase, which in turn depends sensitively on the number of probe photons applied before the $\tilde{\pi}$ pulse in each measurement, we expect a further suppression of any correlated noise below the bound given here.

Derivation of Spin-Flip Terms

This section outlines our derivation of the contributions of incoherent spin flips to the variances $4\Delta S_{z\text{meas}}^2$ and $4\text{Var}(M_1)$ in our noise model above. Both $4\Delta S_{z\text{meas}}^2 = \text{Var}(M_{1+} + M_{1-} - M_{2+} - M_{2-})/2$ and $4\text{Var}(M_1) = \text{Var}(M_{1+} + M_{1-})$ are composed of covariances $\text{Cov}(M_{i\alpha}, M_{j\beta})$ of single-pulse measurement outcomes, where $i, j \in \{1, 2\}$ and $\alpha, \beta \in \{+, -\}$ (see Fig. A5). To evaluate these covariances, we first express each single-pulse measurement $M_{i\alpha}$ as

$$M_{i\alpha} = \frac{\alpha \int_0^T \omega_{i\alpha}(t) dt}{2|d\omega/dN|T}, \quad (8)$$

where $\omega_{i\alpha}(t)$ is the atom-induced cavity shift at a time t from the beginning of pulse $i\alpha$; we here neglect errors in determining the atom-induced cavity shift due to photon shot noise and technical noise, as these are uncorrelated with the atomic state and can be treated separately. In the absence of Raman scattering, each $\omega_{i\alpha}$ is constant in time; and if the spin-echo $\tilde{\pi}$ pulses have perfect fidelity, then $\omega_{i-} = -\omega_{i+}$. Raman scattering and microwave infidelity cause deviations from this ideal behavior, so that

$$\text{Cov}(\omega_{i\alpha}(t), \omega_{j\beta}(t')) \approx \alpha\beta \left| \frac{d\omega}{dN} \right|^2 N_0 [1 - 2r_{i\alpha, j\beta}(t, t')]. \quad (9)$$

Here, for $\alpha = \beta$, we define $r_{i\alpha, j\beta}(t, t')$ as the probability for an atom to be in a different hyperfine state F at time t' of pulse $j\beta$ than at time t of pulse $i\alpha$; for $\alpha = -\beta$, meaning that there is exactly one microwave pulse between t and t' , $r_{i\alpha, j\beta}(t, t')$ is the probability for the hyperfine state to be the same at both times. We have made the approximations that the initial state preparation is projection-noise limited; and that $r_{i\alpha, j\beta}(t, t') \ll 1$, meaning that all the incoherent-spin-flip probabilities—namely, the Raman scattering probabilities $pP_{\Delta F}$, $pP_{\Delta m_F}$, and $pP_{\Delta F\Delta m_F}$ and the microwave infidelity μ —are small. Each expression for $r_{i\alpha, j\beta}(t, t')$ is then, to lowest order, a linear combination of these probabilities with coefficients that depend on how many $\tilde{\pi}$ pulses are applied between pulse $i\alpha$ and pulse $j\beta$. For example, $r_{1-, 1+}(t, t') \approx \frac{t'-t}{2T} pP_{\Delta F} + \frac{t}{2} P_{\Delta m_F} + \frac{t+t'}{2T} pP_{\Delta F\Delta m_F} + \mu$. This expression and similar expressions for the other $r_{i\alpha, j\beta}(t, t')$ are used to evaluate the covariances $\text{Cov}(M_{i\alpha}, M_{j\beta})$ using Eqs. 8 and 9. We thus obtain the terms $(4/3P_{\Delta F} + 1/2P_{\Delta m_F} + 1/3P_{\Delta F\Delta m_F} + \mu)N_0$ in our model for $4\Delta S_{z\text{meas}}^2$ and the terms $(1 - \mu - [2P_{\Delta F}/3 + P_{\Delta m_F}/2 + 2P_{\Delta F\Delta m_F}/3]p)N_0$ in our model for $4\text{Var}(M_1)$.

These results can be understood qualitatively as follows. Incoherent spin flips increase the spin measurement variance $\Delta S_{z\text{meas}}^2 = \text{Var}(M_1 - M_2)/2$ by reducing the correlation between the squeezing and readout measurements M_1 and M_2 . However, they diminish the

projection noise observed in the variance $\text{Var}(M_1)$ of a single measurement, since any scrambling of spins allows the measurement to average over the different ensemble spin states at different times.

B. Derivation of Metrological Squeezing Parameter

In interpreting $\Delta S_{z\text{meas}}^2$ as a measurement uncertainty, and in deriving the quantum uncertainty $[\Delta S_z^2]_{M_1}$ of the state prepared by the squeezing measurement, we make assumptions of uncorrelated noise in the two measurements M_1 and M_2 . These assumptions are justified by the noise model in Sec. A. The dominant noise contributions at the optimum squeezing point—photodetector noise and technical noise attributable to frequency jitter between laser and cavity—are all uncorrelated between the measurements. (Any frequency shaking that is slow enough to be common to both M_1 and M_2 is also common to the cavity shifts ω_+ and ω_- before and after the spin echo and thus does not affect our measurement of $S_z \propto \omega_+ - \omega_-$.) The remaining noise, due to changes in the atomic state via Raman scattering or microwave $\tilde{\pi}$ pulse infidelity, is correlated with the atomic state and hence affects the correlation between the two measurement outcomes. We here generalize the derivation of the conditional spin noise and metrological squeezing parameter to encompass the small effects of such spin-flip noise, thereby fully accounting for all processes in our noise model.

The goal of our analysis is to evaluate $\zeta_m = 2[\Delta S_z^2]_{M_1} S_{\text{in}} / (|\langle \mathbf{S} \rangle|^2)$ using results of our measurements M_1 and M_2 . Since the measurements can change the atomic state, we define S_{zf} as the value of S_z at the end of the first measurement M_1 . The conditional quantum uncertainty $[\Delta S_z^2]_{M_1}$ of the state prepared by the first measurement is found by minimizing $\text{Var}(S_{zf} - wM_1)$ with respect to the weight w given to the measurement information [8, 9]:

$$[\Delta S_z^2]_{M_1} = \min_w \{\text{Var}(S_{zf} - wM_1)\}. \quad (10)$$

The minimum occurs at $w = \text{Cov}(S_{zf}, M_1)/\text{Var}(M_1)$ and is given by [8]

$$[\Delta S_z^2]_{M_1} = \text{Var}(S_{zf}) \left(1 - \frac{\text{Cov}(S_{zf}, M_1)^2}{\text{Var}(S_{zf})\text{Var}(M_1)} \right). \quad (11)$$

As described in Sec. A, the noise in our system is well described by noise that is uncorrelated with S_{zf} and by incoherent spin flips. We begin with the simplifying assumption that all Raman scattering events transfer atoms between the two clock states. In this model, for identical measurements M_1 and M_2 ,

$$\begin{aligned} \text{Cov}(S_{zf}, M_1)^2 &= \text{Cov}(S_{zf}, M_1)\text{Cov}(S_{zf}, M_2) \\ &= \text{Cov}(M_1, M_2)\text{Var}(S_{zf}), \end{aligned} \quad (12)$$

since the only correlations between the two measurements are due to their linear dependence on the common value S_{zf} of S_z at the end of the first measurement and the beginning of the second measurement. Here, $\text{Var}(S_{zf})$ represents the unconditional variance of an ideal, noiseless readout following the squeezing measurement.

We would like to express $\text{Var}(S_{zf})$ in terms of measured quantities. We define $\Delta S_{z\text{meas}}^2 \equiv \text{Var}(M_1 - M_2)/2$ and $\Delta S_{z\text{prep}}^2 \equiv \text{Var}(M_1) - \Delta S_{z\text{meas}}^2 = \text{Cov}(M_1, M_2)$, where the latter equality holds because $\text{Var}(M_1) = \text{Var}(M_2)$. In the limit where the measurement does not change the atomic state and all measurement noise is uncorrelated, $\Delta S_{z\text{prep}}^2$ represents the unconditional variance of S_z , including the CSS projection noise and any technical noise in the initial state preparation. To allow for a measurement that induces spin flips, we use Eq. 12 to relate $\Delta S_{z\text{prep}}^2$ to $\text{Var}(S_{zf})$, obtaining

$$\frac{\Delta S_{z\text{prep}}^2}{\text{Var}(S_{zf})} = \left(\frac{\text{Cov}(M_i, S_{zf})}{\text{Var}(S_{zf})} \right)^2 \equiv (1 - \epsilon_p)^2. \quad (13)$$

To lowest order in the spin-flip probabilities associated with Raman scattering and microwave pulse infidelity, $\epsilon_p \approx pP_{\Delta F} + \mu$. The measured unconditional variance $\Delta S_{z\text{prep}}^2$ is lower than the true variance $\text{Var}(S_{zf})$ by the factor $(1 - \epsilon_p)^2$ because those spins that are flipped part-way through the first measurement contribute less to the measurement (of the time-averaged spin) than to the value S_{zf} at the end of the measurement. Hence,

$$[\Delta S_z^2]_{M_1} = \frac{\Delta S_{z\text{meas}}^2 \Delta S_{z\text{prep}}^2}{(1 - \epsilon_p)^2 (\Delta S_{z\text{prep}}^2 + \Delta S_{z\text{meas}}^2)}. \quad (14)$$

The factor $(1 - \epsilon_p)^2$ has a 0.3 dB effect, smaller than the statistical uncertainty, on the minimum normalized spin noise $\sigma^2 \equiv [\Delta S_z^2]_{M_1} / \Delta S_{z\text{CSS}}^2$, at $p = 6.4(6) \times 10^5$. We do not include this factor in Fig. 3, but we correct for it in reporting the minimum normalized spin noise σ^2 , as well as the entanglement parameter ζ_e at $p = 3 \times 10^5$. We show below that the metrological squeezing parameter ζ_m is independent of ϵ_p .

Note that if we define the measurement strength $\kappa_{\text{meas}} \equiv \Delta S_{z\text{prep}} / \Delta S_{z\text{meas}}$, then for a projection-noise-limited state preparation ($\Delta S_{z\text{prep}}^2 = \Delta S_{z\text{CSS}}^2$) and a measurement that does not change the atomic state ($\epsilon_p = 0$) Eq. 14 reduces to the expression $\sigma^2 = 1/(1 + \kappa_{\text{meas}}^2)$ given by Appel *et al.* [9]. Whereas Appel *et al.* define the measurement strength for a photon-shot-noise-limited measurement, we have here extended the definition to include more general noise.

We wish to determine the metrological squeezing parameter $\zeta_m = 2[\Delta S_z^2]_{M_1} S_{\text{in}} / (|\langle \mathbf{S} \rangle|^2)$ where $|\langle \mathbf{S} \rangle|$ is the length of the mean spin vector at the end of the squeezing measurement. The Rabi oscillation curve from which we obtain the contrast (see Sec. D) is mea-

sured using our standard readout, identical to the squeezing measurement. The contrast $\mathcal{C}(p) = |\langle \mathbf{S} \rangle| / S_0$ that would be observed in an ideal readout of S_{zf} is related to our measured contrast $\mathcal{C}_{\text{meas}}(p)$ by $\mathcal{C}_{\text{meas}}(p) / \mathcal{C}(p) = \text{Cov}(M_2, S_{zf}) / \text{Var}(S_{zf}) = 1 - \epsilon_p$. Hence,

$$\begin{aligned} \zeta_m &= \frac{C_{\text{in}} [\Delta S_z^2]_{M_1}}{\mathcal{C}^2 \Delta S_{z\text{CSS}}^2} \\ &= \frac{C_{\text{in}}}{C_{\text{meas}}^2} \frac{2\Delta S_{z\text{meas}}^2 \Delta S_{z\text{prep}}^2}{S_0 (\Delta S_{z\text{prep}}^2 + \Delta S_{z\text{meas}}^2)}. \end{aligned} \quad (15)$$

The determination of $C_{\text{in}} \equiv S_{\text{in}} / S_0$ is discussed in Sec. D. Using Eq. 15, we obtain the metrological squeezing parameter ζ_m directly in terms of measured variances. Outside this section (B), we do not distinguish between \mathcal{C} and $\mathcal{C}_{\text{meas}}$.

The interesting fact that our evaluation of the metrological squeezing parameter ζ_m , proportional to the squared noise-to-signal ratio, is not affected by photon scattering into free space can be understood as follows: A longer and longer measurement of projection noise fluctuations produced by photon scattering into free space during the measurement, as described by ϵ_p , results in a reduction of the measured spin noise. This would lead one to underestimate the spin noise by a factor $(1 - \epsilon_p)^2$, Eq. 14. However, free-space scattering also reduces the observed contrast, such that the signal-to-noise ratio and the metrological squeezing parameter ζ_m do not depend on ϵ_p .

In the above derivation, we have assumed that all Raman scattering events transfer atoms between the two clock states. Raman scattering out of the clock states introduces a small correction to Eq. 12 and a slight discrepancy between $\text{Var}(M_1)$ and $\text{Var}(M_2)$. A full accounting of the effects of different types of Raman scattering events changes $[\Delta S_z^2]_{M_1}$ by less than 0.1 dB—i.e. less than the least significant figure in our results—at the optimum photon numbers for conditional spin noise reduction and spin squeezing.

C. Spin Noise in Rotated State

In the inset to Fig. 1, we approximate the variance $\Delta S_{z\alpha}^2$ of S_z in a state that has been rotated by an angle α about $\langle \mathbf{S} \rangle$ between the squeezing measurement M_1 and readout measurement M_2 by

$$\Delta S_{z\alpha}^2 \approx \text{Var}(M_1 - M_2)|_{\alpha} - \Delta S_{z\text{meas}}^2, \quad (16)$$

where $\Delta S_{z\text{meas}}^2 = \text{Var}(M_1 - M_2)|_{\alpha=0}/2$. This is a good approximation for all α in the limit where $\Delta S_{z\text{meas}}^2 \ll \Delta S_{z\text{CSS}}^2$ and $\Delta S_{\text{max}} \gg \Delta S_{\text{min}}$.

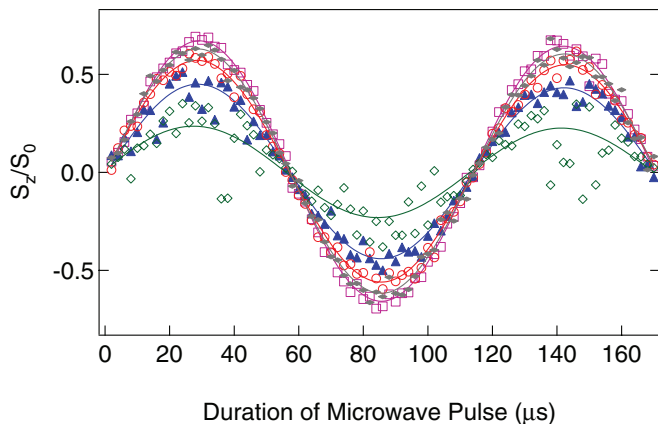


FIG. A6: Measurement of clock contrast. The open squares correspond to the initial contrast with only lock light, the other curves to probe photon numbers between $p = 10^5$ and $p = 9 \times 10^5$.

D. Contrast

To verify and quantify spin squeezing (Fig. 3), we measure the contrast of a Rabi oscillation after the application of probe light (Fig. A6) using an atom number $N_0 = 4.0(1) \times 10^3$. The Rabi oscillation is driven by a microwave pulse of variable duration between the squeezing and readout measurements, during which time both the probe light and the resonator locking light are off.

We observe a contrast loss that is linear in probe photon number p , as well as a process that imparts shot-to-shot phase fluctuations (via imbalances in the intracavity probe power between the two spin echo pulses) and yields a reduction in $|\langle \mathbf{S} \rangle|$ that is quadratic in p . We therefore fit to the data in Fig. 3 the expression $\mathcal{C} = \mathcal{C}_0 \exp(-\alpha p - \beta p^2/2)$, obtaining $\alpha = 7(1) \times 10^{-7}$, $\beta = 9(4) \times 10^{-13}$, and $\mathcal{C}_0 = 0.69(1)$.

As discussed in Sec. B, we define \mathcal{C}_{in} to be the contrast in the ensemble without squeezing ($p=0$) as observed in an ideal readout which flips no spins. By comparing the two probe pulses constituting our real readout measurement, which uses a total of 5×10^5 probe photons, we determine that the reduction in observed contrast due to photon scattering or imperfect microwave rotations during the readout is at most 4(2)%. Correcting for this effect, we obtain $\mathcal{C}_{\text{in}} = 0.71(2)$.

The contrast measurement is performed at lower atom number than the noise measurements in Fig. 3 for two reasons. First, at large atom number, atom projection noise augments the imbalances in intracavity probe power between the spin echo pulses and thus augments the resulting phase fluctuations; this effect can in principle be compensated using the result of the squeezing measurement, but we have not yet done so. Second, at lower atom number, the entire Rabi oscillation curve is in the linear regime of the Lorentzian resonator transmis-

sion profile. We verify that the contrast is independent of atom number by also measuring at $N_0 = 3.5(3) \times 10^4$ the portions of each Rabi oscillation curve that lie in the linear regime of the Lorentzian. A fit to these portions of the curve taken with $p = 0$ (i.e., with lock light only) yields $\mathcal{C}_{\text{in}} = 0.63(6)$. While this measurement incurs greater uncertainty than that at small atom number, it confirms that the contrast is invariant across an order of magnitude in atom number.

VIII. FUNDAMENTAL LIMITS

We outline here a derivation of the fundamental limit on squeezing in our system [10, 11]. A more complete treatment is given by Madsen and Mølmer [10].

An ideal, Heisenberg-area-preserving measurement which adds no noise (i.e. a measurement where the product of squeezing and antisqueezing is unity) can reduce the variance of $N = 2S_z$ by an amount inversely proportional to the broadening it imparts in phase. For our dispersive optical measurement, this broadening comes from the photon shot noise uncertainty on the AC Stark shift due to the probing light. For a given transmitted probe photon number p , the maximum photon-shot-noise-induced phase broadening is achieved by probing on cavity resonance and allows the normalized S_z noise to be reduced to

$$\sigma^2 \equiv \frac{[\Delta S_z^2]_{M_1}}{\Delta S_z^2_{\text{CSS}}} = \frac{1}{1 + N_0 p \phi_{\text{eff}}^2}, \quad (17)$$

where $\phi_{\text{eff}} = \phi_0 \eta_{\text{eff}} / \eta_0$ is the effective phase shift per transmitted photon (see Sec. D). However, our real measurement adds noise because photon scattering can flip the atomic pseudo-spins. Let P_{sc} denote the probability for an atom in a superposition of states $|1\rangle$ and $|2\rangle$ to scatter a photon per probe photon transmitted through the resonator. Then in the large-detuning limit $\delta \gg \Gamma$,

$$\begin{aligned} \phi_{\text{eff}} &= 2 \frac{\delta}{\Gamma} P_{\text{sc}} \\ \Rightarrow N_0 \phi_{\text{eff}}^2 / P_{\text{sc}} &= N_0 \left(\frac{\delta}{\Gamma/2} \right)^2 P_{\text{sc}} = 2N_0 \eta_{\text{eff}}, \end{aligned} \quad (18)$$

since $(2\delta/\Gamma)^2 P_{\text{sc}} = 2\eta_{\text{eff}}$ is the single-atom resonant optical depth (see Sec. A). Thus, Eq. 17 can be expressed in differential form as $d\sigma^2/dp = -2N_0 \eta_{\text{eff}} P_{\text{sc}} (\sigma^2)^2$. The only scattering events which contribute noise are Raman scattering events occurring with probability P_{Ram} per transmitted probe photon. We assume, for simplicity, the worst-case scenario that each Raman-scattered photon transfers an atom from one clock state to the other. Adding the noise contribution from these spin flips and neglecting absorption (which for our largest atom number $N_0 = 33000$ is 0.6%), one obtains [10]

$$\frac{d\sigma^2}{dp} = -2N_0 \eta_{\text{eff}} P_{\text{sc}} (\sigma^2)^2 + 4P_{\text{Ram}}. \quad (19)$$

For $N_0\eta_{\text{eff}} \gg 1$, the normalized spin noise σ^2 has a minimum of

$$\sigma_{\text{min}}^2 = \sqrt{\frac{2}{N_0\eta_{\text{eff}}} \frac{P_{\text{Ram}}}{P_{\text{sc}}}}. \quad (20)$$

In our system $P_{\text{sc}} = 3.0P_{\text{Ram}}$. Thus, for our largest atom number $N_0 = 3.3 \times 10^4$ and our probe polarization and detuning, where $N_0\eta_{\text{eff}} = 3100$, the minimum achievable normalized spin noise is $\sigma_{\text{min}}^2 = -18$ dB.

So far, we have neglected the fundamental contrast loss due to scattering. Including this effect [10], one finds that σ_{min}^2 is reached at $pP_{\text{Ram}} = \frac{\sigma_{\text{min}}^2}{8} \ln(\frac{8}{\sigma_{\text{min}}^2}) = 0.012$ for our system. The associated contrast reduction is only $1 - \mathcal{C} \approx p(\frac{P_{\text{Ray},1} + P_{\text{Ray},2}}{2} - \sqrt{P_{\text{Ray},1}P_{\text{Ray},2}} + P_{\text{Ram}}) = 0.012$, where $P_{\text{Ray},F}$ is the Rayleigh scattering probability in state $|F\rangle$ [12]. Thus, one also obtains a metrological squeezing parameter $\zeta_{\text{m,min}} = \sigma_{\text{min}}^2/\mathcal{C}^2 = -18$ dB. Reaching this fundamental limit would require detection of all the information leaving the resonator (e.g. by performing a phase measurement on resonance [13]) with perfect quantum efficiency and photon-shot-noise-limited sensitivity.

-
- [1] I. Teper, Y. Lin, and V. Vuletić, Phys. Rev. Lett. **97**, 023002 (2006).
- [2] *Technical Information SD-28: Characteristics and Use of Si APD (Avalanche Photodiode)*, Hamamatsu Photonics K.K., Solid State Division (2004), http://sales.hamamatsu.com/assets/applications/SSD/Characteristics_and_use_of_SI_APD.pdf.
- [3] H. K. Cummins, G. Llewellyn, and J. A. Jones, Phys. Rev. A **67**, 042308 (2003).
- [4] V. Vuletić, H. W. Chan, and A. T. Black, Phys. Rev. A **64**, 033405 (2001).
- [5] S. Haroche and J.-M. Raimond, *Exploring the Quantum: Atoms, Cavities, and Photons (Oxford Graduate Texts)* (Oxford University Press, USA, 2006), ISBN 0198509146.
- [6] N. F. Ramsey, Phys. Rev. **78**, 695 (1950).
- [7] L. M. K. Vandersypen and I. L. Chuang, Rev. Mod. Phys. **76**, 1037 (2005).
- [8] G. Leuchs, C. Silberhorn, F. König, P. K. Lam, A. Sizmann, and N. Korolkova, in *Quantum information with continuous variables*, edited by S. L. Braunstein and A. K. Pati (Kluwer Academic, Norwell, MA, 2003), pp. 379–421.
- [9] J. Appel, P. Windpassinger, D. Oblak, U. Hoff, N. Kjaergaard, and E. S. Polzik, Proceedings of the National Academy of Sciences **106**, 10960 (2009).
- [10] L. B. Madsen and K. Mølmer, Phys. Rev. A **70**, 052324 (2004).
- [11] K. Hammerer, K. Mølmer, E. S. Polzik, and J. I. Cirac, Phys. Rev. A **70**, 044304 (2004).
- [12] R. Ozeri, C. Langer, J. D. Jost, B. DeMarco, A. Ben-Kish, B. R. Blakestad, J. Britton, J. Chiaverini, W. M. Itano, D. B. Hume, et al., Phys. Rev. Lett. **95**, 030403 (2005).
- [13] I. Teper, G. Vrijsen, J. Lee, and M. A. Kasevich, Phys. Rev. A **78**, 051803(R) (2008).